Nature of low-lying electric dipole resonance excitations in ^{74}Ge

D. Negi,[1,2,*] M. Wiedeking,[1,†] E. G. Lanza,[3] E. Litvinova,[4,5] A. Vitturi,[6,7] R. A. Bark,[1] L. A. Bernstein,[8,9] D. L. Bleuel,[8] S. Bvumbi,[10] T. D. Bucher,[1] B. H. Daub,[8,9] T. S. Dinoko,[1,11] J. L. Easton,[1,11] A. Görgen,[12] M. Guttormsen,[12] P. Jones,[1] B. V. Kheswa,[1,13] N. A. Khumalo,[11,14] A. C. Larsen,[12] E. A. Lawrie,[1] J. J. Lawrie,[1] S. N. T. Majola,[1,15] L. P. Masiteng,[10] M. R. Nchodu,[1] J. Ndayishimye,[1,13] R. T. Newman,[13] S. P. Noncolela,[1,11] J. N. Orce,[11] P. Papka,[1,13] L. Pellegri,[1,16] T. Renstrøm,[12] D. G. Roux,[17] R. Schwengner,[18] O. Shirinda,[1,13] and S. Siem[12]

[1]*iThemba LABS, P.O. Box 722, Somerset West 7129, South Africa*
[2]*UM-DAE Centre for Excellence in Basic Sciences, Mumbai 400098, India*
[3]*INFN, Sezione di Catania, I-95123 Catania, Italy*
[4]*Western Michigan University, Kalamazoo, Michigan 49008-5252, USA*
[5]*National Superconducting Cyclotron Laboratory, Michigan State University, East Lansing, Michigan 48824-1321, USA*
[6]*Dipartimento di Fisica e Astronomia, Università di Padova, Italy*
[7]*INFN, Sezione di Padova, I-35131 Padova, Italy*
[8]*Lawrence Livermore National Laboratory, Livermore, California 94550-9234, USA*
[9]*University of California, Berkeley, California 94720-1730, USA*
[10]*University of Johannesburg, Auckland Park 2006, South Africa*
[11]*University of the Western Cape, Bellville 7535, South Africa*
[12]*Department of Physics, University of Oslo, N-0316 Oslo, Norway*
[13]*Department of Physics, Stellenbosch University, Matieland 7602, South Africa*
[14]*University of Zululand, KwaDlangezwa 3886, South Africa*
[15]*University of Cape Town, Rondebosch 7701, South Africa*
[16]*University of the Witwatersrand, Johannesburg 2050, South Africa*
[17]*Rhodes University, Grahamstown 6410, South Africa*
[18]*Helmholtz-Zentrum Dresden-Rossendorf, 01328 Dresden, Germany*

(Received 11 September 2015; revised manuscript received 25 February 2016; published 23 August 2016)

Isospin properties of dipole excitations in ^{74}Ge are investigated using the $(\alpha,\alpha'\gamma)$ reaction and compared to (γ,γ') data. The results indicate that the dipole excitations in the energy region of 6 to 9 MeV adhere to the scenario of the recently found splitting of the region of dipole excitations into two separated parts: one at low energy, being populated by both isoscalar and isovector probes, and the other at high energy, excited only by the electromagnetic probe. Relativistic quasiparticle time blocking approximation (RQTBA) calculations show a reduction in the isoscalar $E1$ strength with an increase in excitation energy, which is consistent with the measurement.

DOI: 10.1103/PhysRevC.94.024332

I. INTRODUCTION

In recent years there has been a surge in experimental studies of dipole excitations lying on the low-energy tail of the isovector giant dipole resonance, the so-called pygmy dipole resonance (PDR). The PDR has been interpreted as an exotic mode of excitation due to the motion of a weakly bound neutron excess against an almost inert proton-neutron core [1–3], although single particle-hole excitations are also considered [4,5]. One major reason for the renewed interest in the PDR is the possibility of carrying out high-resolution measurements on these low-lying dipole excitations using heavy ion [6,7], proton [8,9], and α inelastic scattering experiments [10,11]. An experimental technique, combining particle and γ-ray detection techniques, to study the response of dipole excitations to isoscalar probes was pioneered by Poelhekken *et al.* [12] and applied in several studies since [6,7,10,11,13–17]. These experiments provide complementary information to those obtained from (γ,γ') experiments which investigate the isovector nature of the excitations [18–24]. One of the surprising results from recent experiments is the isospin splitting of the PDR [2,3,10,11,13]. This provides intimate knowledge about the isospin nature of these excitations which would not be possible to infer from (γ,γ') experiments alone. These experimental discoveries were followed by intensive theoretical investigations [25–30].

Incidentally, scattering experiments with isocalar probes for the study of the PDR have so far been limited to only certain regions of the nuclear chart and carried out mainly on nuclei with large neutron-to-proton ratios [6,10,13,14,17]. Information on how the results from scattering reactions compare to those of (γ,γ') experiments in nuclei closer to $N/Z = 1$ are also becoming available [7,12,15,16]. Since most of the incident isoscalar probes are sensitive to the surface of the nucleus, the information gathered advances our understanding of the evolution of the PDR with changing N/Z. This information is extrapolated for obtaining better estimates of the total strength exhausted by the PDR in nuclei of astrophysical importance, many of which are still inaccessible with the available experimental facilities and techniques. The PDR has been suggested to have a significant

*dinphysics@gmail.com
†wiedeking@tlabs.ac.za

impact on neutron capture rates and isotopic solar abundance distributions in r-process nucleosynthesis [31–34]. Further, the PDR could possibly constrain the equation of state of hot and dense neutron matter as found in neutron star remnants [35,36].

In this contribution, we present results on ^{74}Ge where a high-resolution measurement was carried out using the α inelastic scattering reaction. In its ground state, ^{74}Ge is a moderately deformed prolate nucleus [37,38] with $N/Z = 1.32$. For comparison and to facilitate the discussion, information about the $E1$ strength distribution is also available from (γ,γ') data in ^{74}Ge [39,40].

II. EXPERIMENTAL DETAILS

The experiment was performed at the Separated Sector Cyclotron facility at iThemba Laboratories with the AFRican Omnipurpose Detector for Innovative Techniques and Experiments (AFRODITE) γ-ray detector array[41] in conjunction with two identical particle telescopes, each of them consisting of two silicon detectors (in ΔE-E configuration). The α particles with a beam energy of 48 MeV impinged on a 500 μg/cm^2 thick ^{74}Ge target to populate excited states in the inelastic scattering reaction. The experiment was carried out over a period of five days with an average beam current of $\sim$14 particle nA. The telescopes were placed at an angle of $\theta = \pm 45^\circ$ with respect to the beam axis. The dimensions of the W1-type double-sided silicon strip detectors [42] were 5 cm $\times$ 5 cm and they consisted of 16 parallel and perpendicular strips 3 mm wide. The distance from target to the telescopes was 5 cm, yielding an angular range of 20° to 72° in the laboratory frame of reference. Thicknesses of the ΔE and E detectors were 284 and 1000 μm, respectively, and to suppress δ electrons an aluminum foil of 4.1 mg/cm^2 areal density was placed in front of the ΔE detectors. Calibration of individual strips of the silicon detectors was performed using a ^{228}Th α source.

AFRODITE, at the time of the experiment, consisted of nine Clover HPGe detectors with four detectors at 135° and five at 90° at a distance of 19.6 cm from the target. The detectors were calibrated using standard ^{152}Eu and ^{56}Co sources. High γ-ray energy efficiency parameters for the AFRODITE array were available from Ref. [41]. XIA digital electronics [43] was used to acquire time-stamped online data in singles mode.

III. DATA ANALYSIS

From the time-stamped data, events with single-, double-, and higher fold coincidences were constructed with an offline coincidence time window of 600 ns. From double-fold events, the α-γ coincidences were extracted by placing a gate on the α particles in the particle identification spectrum. A projection of α-γ coincidences onto the α-particle axis is shown in Fig. 1. The selection of correlated events was made with a coincidence time of less than 140 ns by placing appropriate gates around the prompt time peak. Uncorrelated event contributions were extracted and subtracted from the data by placing off-prompt time gates to the early and late sides of the prompt timing peak.

Kinematic corrections due to the recoil energy of ^{74}Ge and the energy losses of scattered α particles in the target and aluminum foils were applied to the α particles. Although the target contained some oxygen and carbon contaminants, the recoil corrections for the scattered α particles from ^{74}Ge are quite different compared to those of light contaminant nuclei, thereby allowing a clean extraction of the events of interest. For instance, the corrections from ^{74}Ge versus ^{16}O differ by $\sim$1 and $\sim$10 MeV at 20° and 72° detection angles, respectively. The energy resolution of the ΔE-E telescopes, measured from the elastic peak, was $\approx$250 keV. Despite the low velocities of the ^{74}Ge recoils, corrections for Doppler effects of the high-energy γ rays were found to be necessary and useful.

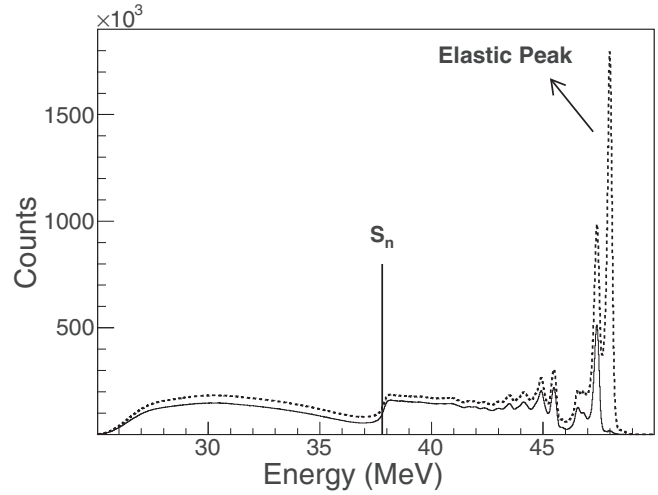

FIG. 1. Spectrum of α particles detected in coincidence with γ rays. Solid and dashed curves are representing data with and without the subtraction of uncorrelated events, respectively. Visible peaks (solid curve) are strongly populated discrete states in ^{74}Ge. S_n indicates the location of the neutron separation energy.

Transitions (E_γ) to the ground state were extracted with the condition $|E_\gamma - E_x| \leqslant 130$ keV imposed on the α-γ coincidence events, where E_x refers to the excitation energy of the decaying state and is determined from the energy of the scattered α particles. Placing this stringent energy requirement upon the data, together with the differences in kinematic properties, ensures that only transitions from ^{74}Ge are extracted, eliminating contributions due to contaminants.

Additionally, various combinations of angles between the direction of the recoiling nuclei (as defined by the α particles detected in the particle telescope) and the γ rays detected in the Clover detectors were used for the determination of angular distributions.

IV. RESULTS AND DISCUSSION

The spectrum of direct γ-ray transitions to the ground state is shown in Fig. 2, where in addition to many states for $E_x < 6$ MeV, a high concentration of states and strength is also observed for $6.5 < E_x < 8$ MeV. Although the overall sensitivity to high-energy transitions is relatively poor, many transitions observed in (γ,γ') experiments [39,40] can also be clearly identified in the present data. Unresolved strength was separated from intensities of individual transitions by simultaneously fitting the peaks using the ROOT analysis

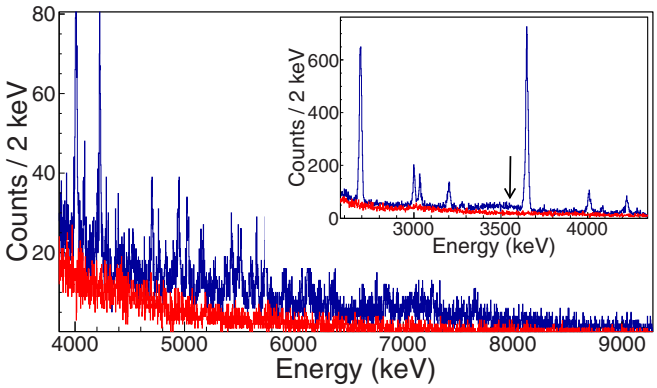

FIG. 2. Spectrum of γ-ray transitions decaying directly to the ground state from defined excitation energies. Blue and red spectra correspond to correlated and uncorrelated events, respectively. Inset: the lower energy part of the spectrum where the arrow indicates the position of the unobserved 3558-keV transition, known from (γ,γ') experiments [39,40].

package [44] in a 16-keV per channel compressed γ-ray spectrum. The unresolved, underlying intensity for $6.5 < E_x < 8$ MeV amounts to ≈50%. Comparisons with the recent (γ,γ') measurement [40] reveal several states which were not populated in the $(\alpha,\alpha'\gamma)$ reaction but are observed in the (γ,γ') measurement. However, the states at $E_x = 6850$ and 7060 keV are populated only through the $(\alpha,\alpha'\gamma)$ reaction.

The multipole nature of the high-energy transitions was determined through angular distribution measurements, shown in Fig. 3. Because of the paucity of the data, the angular distribution was extracted simultaneously for the total (resolved and unresolved) γ-ray strength in the interval $6.5 < E_x < 8$ MeV. For comparison, angular distributions of known dipole ($E_\gamma =$ 2690 keV and $E_\gamma =$ 3648 keV) and quadrupole transitions ($E_\gamma = 596$ keV) in ^{74}Ge are also included in Fig. 3. Although the $6.5 < E_x < 8$ MeV strength does not exhibit a perfect agreement with the expected distribution of a dipole transition, the similarity to the two known dipole transitions strongly supports the overall dipole nature. Natural-parity states are preferentially populated in this reaction [45], leading to an assignment of spin parity $J^\pi = 1^-$ to the decaying states.

In Fig. 4(a), relative cross sections of observed $J^\pi = 1^-$ states are plotted and normalized to the 4007-keV state. For comparison, Fig. 4(b) displays relative integrated scattering cross sections (I_s) from (γ,γ') data [40], where the 4007-keV state is taken as the reference once again. All states for $E_x >$ 6 MeV from the (γ,γ') data are assumed to have negative parity and are plotted in Fig. 4, whereas in both panels only states have been included with known negative-parity for $E_x <$ 6 MeV, as deduced from the (γ,γ') data. An exception are the states at 2690, 3033, and 3648 keV with assigned $J^\pi =$ $1,1,1^+$, respectively [39]. The $J^\pi = 1^+$ assignment to the 3648-keV state is based on a polarization measurement [39]. However, this state has also been observed in an earlier (α,α') work [46]. Since inelastic α-scattering populates preferentially natural-parity states, the observed strong cross section in the present experiment contradicts this assignment. Hence, the transition is assumed to be electric dipole in character. Similar

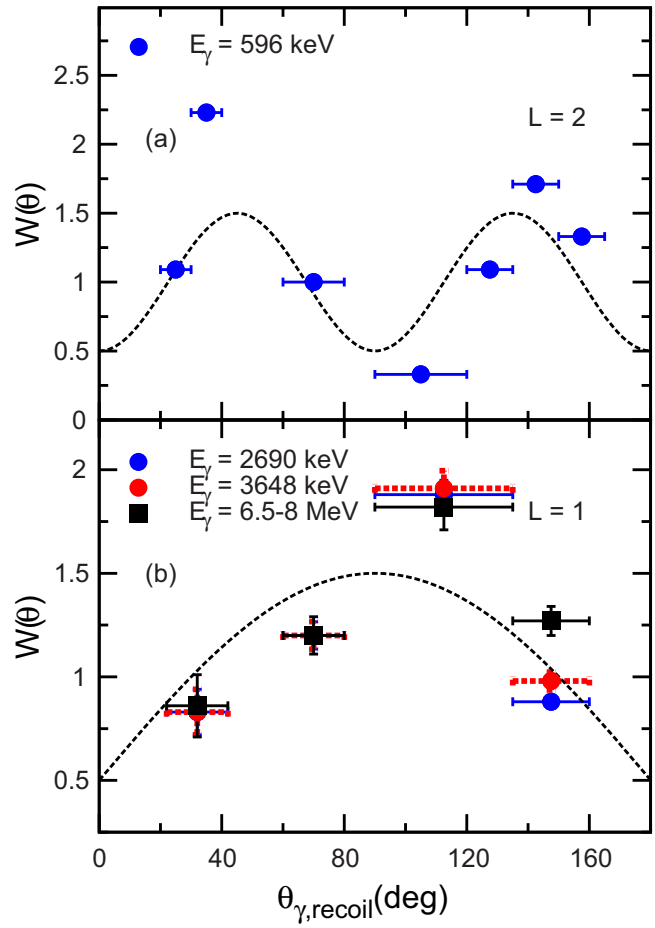

FIG. 3. Angular distributions of (a) the first-excited state $l = 2$ 596-keV transition and (b) $l = 1$ transitions from the known 2690- and 3648-keV states together with the total strength of resolved and unresolved transitions for $6.5 < E_x < 8$ MeV in ^{74}Ge.

considerations are applied to the 2690- and 3033-keV states. The complete absence of the 3558-keV state in the present data (see arrow in inset of Fig. 2) is noteworthy, since this state has been observed in the (γ,γ') work and was assigned $J^\pi = 1^{(-)}$ [39].

The comparison shows the presence of two different regions in the energy range of the investigated dipole excitations. In the lower part ($3 < E_x < 6$ MeV) the excitations due to $(\alpha,\alpha'\gamma)$ are enhanced compared to the upper part ($6 < E_x < 9$ MeV). For (γ,γ') excitations the trend is reversed, indicating a dominant isovector nature of the higher-energy dipole excitations. This reduction in relative cross section in the $(\alpha,\alpha'\gamma)$ data becomes even more pronounced if the intensity of the 3648-keV state is taken as a normalization reference.

The reduction of cross sections in the $(\alpha,\alpha'\gamma)$ data for states $E_x > 6$ MeV, compared to cross sections for $E_x < 6$ MeV, is larger than observed in previous cases. Indeed, with respect to $(\alpha,\alpha'\gamma)$ studies on ^{140}Ce, ^{138}Ba, and ^{124}Sn [10,11,13], the isoscalar response at low energies (<6 MeV) is much stronger. The current result shows that many of the dipole excitations in the $6 < E_x < 9$ MeV range in ^{74}Ge are mixed with larger isovector components. However, a few weakly populated pure

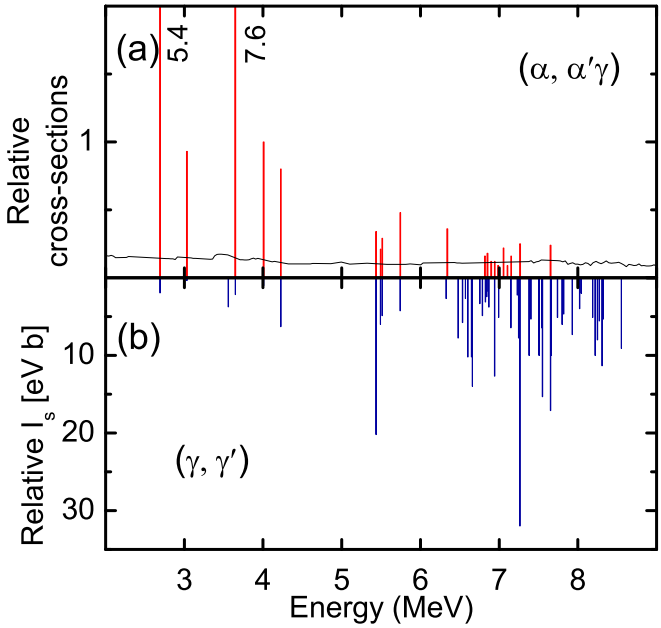

FIG. 4. In panel (a) relative cross sections of $E1$ transitions from the $(\alpha,\alpha'\gamma)$ data are plotted, while in panel (b) the relative integrated scattering cross sections I_s obtained from (γ,γ') data [40] are shown. Numbers next to some transitions indicate the total value of relative cross section. In panel (a), the sensitivity limit is shown by the black solid curve and was determined using the procedure outlined in Ref. [11]. Uncertainties on the cross sections in panel (a) are ∼50% for weakly populated states and decrease to ∼15% for strongly populated states.

isoscalar states, as well as several pure isovector states, are found for $E_x > 6$ MeV. These results indicate that the dipole excitations in ^{74}Ge for $E_x > 6$ MeV do show the common scenario of dipole excitations splitting in two distinct parts: one at lower energy, whose states have a strong isospin mixing, and one at higher energy with predominant isovector character.

We have performed calculations of the dipole transition densities in ^{74}Ge within the relativistic quasiparticle time blocking approximation (RQTBA) [47] based on the covariant energy density functional theory (CEDFT) [48,49]. The RQTBA has been developed to include spreading mechanisms, other than Landau damping [one-particle–one-hole (1p1h) or two-quasiparticle (2q) configurations] into the microscopic description of nuclear excitation modes within the relativistic framework. The existing versions of RQTBA include 2q ⊗ phonon [47] or two-phonon [50,51] configurations in a fully self-consistent way. Parameters (in the present version with the NL3* [52] interaction, 8 parameters) of the CEDFT were fixed by fitting masses and radii of several characteristic nuclei throughout the nuclear chart [49] and no adjustments were involved in the subsequent calculations.

The calculations were performed in the following three steps: (i) the single-particle spectrum was obtained from the self-consistent relativistic mean-field solution; (ii) the phonon spectrum was computed by the self-consistent relativistic quasiparticle random-phase approximation (RQRPA), and (iii) the Bethe-Salpeter equation for the nuclear dipole response was solved within the RQTBA employing the RQRPA

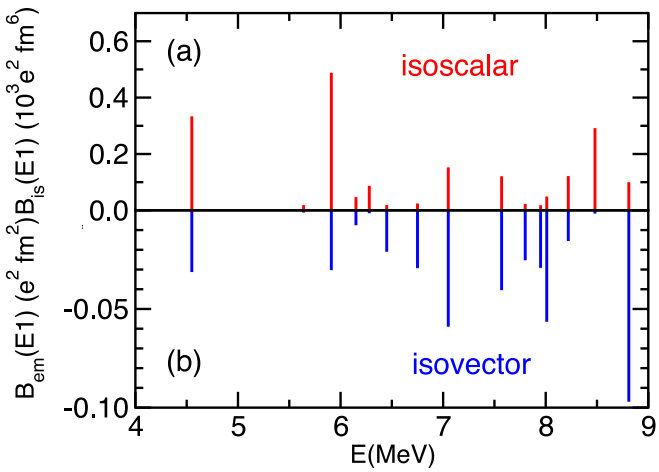

FIG. 5. Reduced transition probabilities in ^{74}Ge from RQTBA calculations plotted for the isoscalar (a) and electromagnetic (isovector) (b) dipole operators.

phonons to construct the induced energy-dependent residual interaction. The low-energy region of the dipole spectrum is calculated with the RQTBA. It includes mixing of quasiparticles with phonons, in particular, with the lowest 2^+ collective state obtained in RQRPA at $E_x \sim 0.6$ MeV and the lowest 3^- state at $E_x \sim 3.4$ MeV, while without mixing there is no dipole strength at the energies of interest. The phonon spectra are consistent with experimental observations for the first-excited 2^+ and 3^- states at 596 and 2536 keV [53]. Reduced transition probabilities from RQTBA calculations with 25-keV smearing (bunching) for isoscalar and isovector dipole operators are plotted in Figs. 5(a) and 5(b). Although these calculations also suggest a suppression in the isoscalar $E1$ strength at higher energies, they underestimate the experimentally observed suppression in ^{74}Ge.

Figure 6 shows the proton, neutron, isoscalar, and isovector transition densities for calculated states at $E_x = 4.55$ and 7.05 MeV. The lower-lying state [Fig. 6(a)] exhibits the usual pattern for an almost pure isoscalar dipole state, with the proton and neutron transition densities in phase inside the nucleus and at the nuclear surface. Consequently, the isoscalar transition density has a pattern typical of the compressional mode with a node close to the nuclear surface. In contrast, the higher-lying state [Fig. 6(b)] exhibits the typical behavior

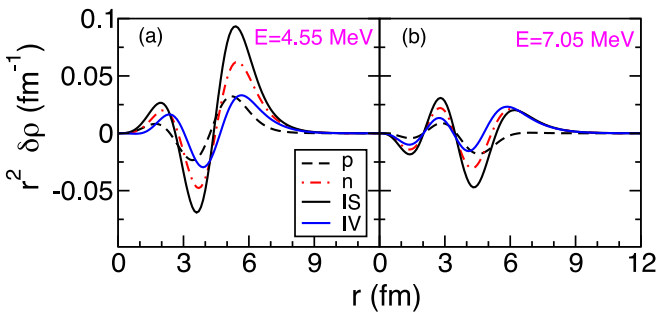

FIG. 6. Transition densities for two calculated RQTBA states at $E_x = 4.55$ (a) and 7.05 MeV (b) in ^{74}Ge.

of a pygmy dipole state where the proton and neutron transition densities are in phase inside the nucleus, while at the surface region the contribution comes from the neutron density only. Consequently, at the surface the isoscalar and isovector transition densities have the same intensity, giving rise to a strong isospin mixing. For the calculated dipole states this behavior is supported by the present data, which manifest significant isospin mixing in the energy region under investigation.

An estimate of the inelastic cross section of states due to different reaction mechanisms is obtained using the TALYS 1.6 reaction code [54]. These calculations suggest that for a 48-MeV α beam, the compound reaction does not contribute at any excitation energy under consideration, while for $E_x \approx$ 6 MeV the contribution from pre-equilibrium reactions is an order of magnitude less than that from direct reactions and gradually increases with E_x. Therefore, a direct comparison with other experimental data should be taken with some degree of caution at the highest excitation energies.

In principle, the presence of the Coulomb interaction between the target and projectile has the capability to substantially contribute to the observed cross sections [55]. To investigate the effect of the Coulomb interaction on the observed inelastic cross sections, theoretical cross sections were calculated both with and without taking the Coulomb interaction into account. These theoretical cross sections were obtained for the dipole states at $E_x = 4.55$ and 7.05 MeV by performing distorted wave Born approximation (DWBA) calculations, carried out using the FRESCO code [56]. The radial nuclear form factors were constructed within a double-folding procedure using the microscopic transition densities of Fig. 6; see Ref. [57] for more details on the procedure. For the Coulomb form factors we have used the analytic expression built inside the FRESCO code. For these calculations the double-folding potential was used as the real part of the optical potential, while for the imaginary part the same geometry as for the real part but with half the intensity was chosen [57]. These results are shown in Fig. 7 where a negligible difference between the calculations performed using only the nuclear interaction (red curve) and using both the nuclear and Coulomb interaction (blue curve) is observed for the detection angles under study (blue shaded areas). For these low-lying dipole states it has been shown that the nuclear and Coulomb contributions interfere constructively in the nuclear surface region [55]. This feature is expected not to be visible for this relatively low incident energy since the Coulomb contribution becomes important as the beam energy increases towards 30 MeV/u [55,58]. We are aware of the fact that, while the relation between the inelastic cross section and the $B_{\rm em}(E1)$ is clear for the Coulomb excitation (they are proportional), the relation between the isoscalar response and the inelastic excitation cross section due to an isoscalar probe is not so evident. In fact, the ratio between the $B_{\rm is}(E1)$ of the two states at 4.55 and 7.05 MeV is 2.2, while the ratio between the corresponding values of the cross sections is 6.4 at the first maximum. If we eliminate the effect of the Q value, by placing the two states at the same energy, then the ratio decreases to 4.1, still far from 2.2. However, in Ref. [55] a calculation of the cross section was presented in the framework of a semiclassical model, that provides the missing link to directly compare the results from the microscopic RQTBA calculations to experimental data measured via the $(\alpha,\alpha'\gamma)$ reaction, confirming the structural splitting of the low-lying $E1$ strength.

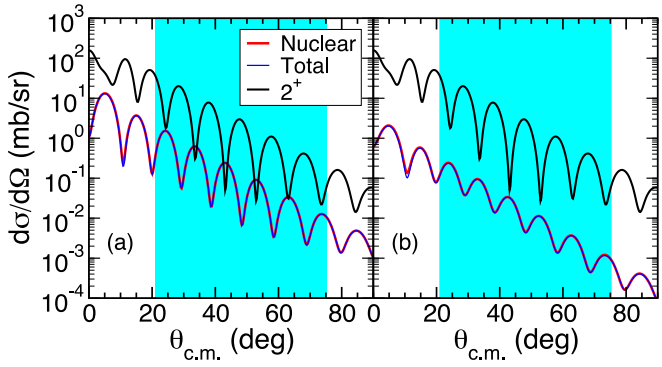

FIG. 7. Cross sections of inelastic scattering of α particles are plotted as a function of scattering angle in the center-of-mass frame for the 2^+ state in ^{74}Ge at 596 keV and dipole states at (a) 4.55 and (b) 7.05 MeV. The blue shaded areas represent the angular coverage of scattered α particles in the present measurement.

It is instructive to also have an estimate of the cross section of states with higher multipolarities. Therefore, we also performed calculations for the first-excited 2^+ state in ^{74}Ge, using a collective macroscopic nuclear form factor. The $B(E2)$ value of the 596-keV transition is taken to be 3050 e^2 fm^4 from Ref. [59] with a deformation length of 1.43 fm. The results are shown in Fig. 7, where the cross sections for the 2^+ state (black curve) are significantly higher when compared to the dipole states. This is not only the case for the detection angles of the present experiment but also for very forward angles.

It is interesting to point to a recent measurement of the photon strength function below the neutron separation energy in ^{74}Ge [60], using the so-called Oslo method. Despite the limited γ-ray detection resolution, a broad structure is observed in the $6 < E_\gamma < 8$ MeV range. It is highly probable that this feature is the same pygmy dipole resonance structure as observed in this work.

V. SUMMARY AND CONCLUSION

We provide new results, which indicate a suppression in relative cross section for the excitation of the PDR in ^{74}Ge populated through inelastic α scattering, when compared to photon scattering data for $E_x > 6$ MeV. The observed dipole response splits into two distinct parts: one at lower energy, with excitations that have strong isospin mixing, and one at higher energy, with predominant isovector character. The results are particularly important in improving our understanding of the emergence and persistence of the PDR for low N/Z nuclei. As such, measurements in other mass regions are undoubtedly necessary to fully understand the evolution of the PDR from near-isospin saturated systems towards nuclei with large N/Z ratios. Finally, the present work highlights the importance of using complementary probes to photon scattering, in order

to reveal detailed information about the underlying nature of dipole excitations.

ACKNOWLEDGMENTS

The authors would like to thank the operational staff at iThemba LABS for providing excellent beam quality throughout the experiment and Lawrence Berkeley National Laboratory for making available the ^{74}Ge target. This work was supported by the National Research Foundation of South Africa under Grants No. 92789, and No. 93500; by the Research Council of Norway, Project Grants No. 205528, No. 213442, and No. 210007; by US-NSF Grants No. PHY-1204486 and No. PHY-1404343; by the US Department of Energy under Contracts No. DE-AC52-07NA27344, and No. DE-AC02-05CH11231; and by ERC-STG-2014 Grant No. 637686.

[1] N. Paar, D. Vretenar, E. Khan, and G. Colò, Rep. Prog. Phys. **70**, 691 (2007).
[2] D. Savran, T. Aumann, and A. Zilges, Prog. Part. Nucl. Phys. **70**, 210 (2013).
[3] A. Bracco, F. C. L. Crespi, and E. G. Lanza, Eur. Phys. J. A **51**, 99 (2015).
[4] A. M. Lane, Ann. Phys. **63**, 171 (1971).
[5] P.-G. Reinhard and W. Nazarewicz, Phys. Rev. C **87**, 014324 (2013).
[6] L. Pellegri *et al.*, Phys. Lett. B **738**, 519 (2014).
[7] F. C. L. Crespi *et al.*, Phys. Rev. C **91**, 024323 (2015).
[8] I. Poltoratska *et al.*, Phys. Rev. C **85**, 041304(R) (2012).
[9] A. M. Krumbholz *et al.*, Phys. Lett. B **744**, 7 (2015).
[10] D. Savran *et al.*, Phys. Rev. Lett. **97**, 172502 (2006).
[11] J. Endres *et al.*, Phys. Rev. C **80**, 034302 (2009).
[12] T. D. Poelhekken *et al.*, Phys. Lett. B **278**, 423 (1992).
[13] J. Endres *et al.*, Phys. Rev. Lett. **105**, 212503 (2010).
[14] V. Derya *et al.*, J. Phys. Conf. Ser. **366**, 012012 (2012).
[15] V. Derya *et al.*, Nucl. Phys. A **906**, 94 (2013).
[16] V. Derya *et al.*, Phys. Lett. B **730**, 288 (2014).
[17] F. C. L. Crespi *et al.*, Phys. Rev. Lett. **113**, 012501 (2014).
[18] S. Volz *et al.*, Nucl. Phys. A **779**, 1 (2006).
[19] K. Govaert *et al.*, Phys. Rev. C **57**, 2229 (1998).
[20] C. Romig *et al.*, Phys. Rev. C **88**, 044331 (2013).
[21] T. Shizuma *et al.*, Phys. Rev. C **78**, 061303 (2008).
[22] R. Schwengner *et al.*, Phys. Rev. C **76**, 034321 (2007).
[23] N. Benouaret *et al.*, Phys. Rev. C **79**, 014303 (2009).
[24] A. Makinaga *et al.*, Phys. Rev. C **82**, 024314 (2010).
[25] N. Tsoneva and H. Lenske, Phys. Rev. C **77**, 024321 (2008).
[26] N. Paar, Y. F. Niu, D. Vretenar, and J. Meng, Phys. Rev. Lett. **103**, 032502 (2009).
[27] M. Martini, S. Péru, and M. Dupuis, Phys. Rev. C **83**, 034309 (2011).
[28] M. Tohyama and T. Nakatsukasa, Phys. Rev. C **85**, 031302(R) (2012).
[29] D. Vretenar, Y. F. Niu, N. Paar, and J. Meng, Phys. Rev. C **85**, 044317 (2012).
[30] H. Nakada, T. Inakura, and H. Sawai, Phys. Rev. C **87**, 034302 (2013).
[31] S. Goriely, Phys. Lett. B **436**, 10 (1998).
[32] S. Goriely, E. Khan, and M. Samyn, Nucl. Phys. A **739**, 331 (2004).
[33] E. Litvinova *et al.*, Nucl. Phys. A **823**, 26 (2009).
[34] I. Daoutidis and S. Goriely, Phys. Rev. C **86**, 034328 (2012).
[35] J. Piekarewicz, Phys. Rev. C **73**, 044325 (2006).
[36] J. Piekarewicz, Phys. Rev. C **83**, 034319 (2011).
[37] L. Rosier and E. I. Obiajunwa, Nucl. Phys. A **500**, 323 (1989).
[38] P. Möller *et al.*, At. Data Nucl. Data Tables **94**, 758 (2008).
[39] A. Jung *et al.*, Nucl. Phys. A **584**, 103 (1995).
[40] R. Massarczyk *et al.*, Phys. Rev. C **92**, 044309 (2015).
[41] M. Lipoglavšek *et al.*, Nucl. Instrum. Methods Phys. Res., Sect. A **557**, 523 (2007).
[42] Mircon Semiconductor, Product Cataloque, http://www.micronsemiconductor.co.uk/pdf/w1.pdf.
[43] http://www.xia.com.
[44] https://root.cern.ch.
[45] W. W. Eidson and J. G. Cramer, Jr., Phys. Rev. Lett. **9**, 497 (1962).
[46] B. Schürmann *et al.*, Nucl. Phys. A **475**, 361 (1987).
[47] E. Litvinova, P. Ring, and V. Tselyaev, Phys. Rev. C **78**, 014312 (2008).
[48] P. Ring, Prog. Part. Nucl. Phys. **37**, 193 (1996).
[49] D. Vretenar *et al.*, Phys. Rep. **409**, 101 (2005).
[50] E. Litvinova, P. Ring, and V. Tselyaev, Phys. Rev. Lett. **105**, 022502 (2010).
[51] E. Litvinova, P. Ring, and V. Tselyaev, Phys. Rev. C **88**, 044320 (2013).
[52] G. A. Lalazissis *et al.*, Phys. Lett. B **671**, 36 (2009).
[53] http://www.nndc.bnl.gov (as of April 2015).
[54] A. J. Koning *et al.*, *Nuclear Data for Science and Technology*, edited by O. Bersillon *et al.* (EDP Sciences, Nice, France, 2008), p. 211 (see also http://www.talys.eu).
[55] E. G. Lanza, A. Vitturi, E. Litvinova, and D. Savran, Phys. Rev. C **89**, 041601(R) (2014).
[56] I. J. Thompson, Comput. Phys. Rep. **7**, 167 (1988); http://www.fresco.org.uk.
[57] E. G. Lanza, A. Vitturi, and M. V. Andrés, Phys. Rev. C **91**, 054607 (2015).
[58] E. G. Lanza, A. Vitturi, M. V. Andres, F. Catara, and D. Gambacurta, Phys. Rev. C **84**, 064602 (2011).
[59] R. Lecomte, M. Irshad, S. Landsberger, G. Kajrys, P. Paradis, and S. Monaro, Phys. Rev. C **22**, 2420 (1980).
[60] T. Renstrøm *et al.*, Phys. Rev. C **93**, 064302 (2016).